Published in final edited form as:
J Mater Sci Mater Med. 2012 September ; 23(9): 2115–2126. doi:10.1007/s10856-012-4691-6.

Direct Scaffolding of Biomimetic Hydroxyapatite-gelatin Nanocomposites using Aminosilane Cross-linker for Bone Regeneration

Chi-Kai Chiu[1], **Joao Ferreira**[2], **Tzy-Jiun M. Luo**[1], **Haixia Geng**[2,3], **Feng-Chang Lin**[4], and **Ching-Chang Ko**[2,5,6,*]

[1]Department of Materials Science and Engineering, EBI 3002, North Carolina State University, Raleigh, NC 27606, US

[2]Oral Biology Program, School of Dentistry, University of North Carolina, CB #7454, Chapel Hill, NC 27599, US

[3]Dental School of Jining Medical College, Jining, China

[4]Department of Biostatistics, University of North Carolina, Chapel Hill, US

[5]Department of Orthodontics, School of Dentistry, University of North Carolina, CB #7454, Chapel Hill, NC 27599, US

[6]Applied and Materials Science Program, University of North Carolina, Chapel Hill, NC 27599, US

Abstract

Hydroxyapatite-gelatin modified siloxane (GEMOSIL) nanocomposite was developed by coating, kneading and hardening processes to provide formable scaffolding for alloplastic graft applications. The present study aims to characterize scaffolding formability and mechanical properties of GEMOSIL, and to test the *in vitro* and *in vivo* biocompatibility of GEMOSIL. Buffer Solution initiated formable paste followed by the sol-gel reaction led to a final hardened composite. Results showed the adequate coating of aminosilane, 11–19 wt%, affected the cohesiveness of the powders and the final compressive strength (69 MPa) of the composite. TGA and TEM results showed the effective aminosilane coating that preserves hydroxyapatite-gelatin nanocrystals from damage. Both GEMOSIL with and without titania increased the mineralization of preosteoblasts *in vitro*. Only did titania additives revealed good *in vivo* bone formation in rat calvarium defects. The scaffolding formability, due to cohesive bonding among GEMOSIL particles, could be further refined to fulfill the complicated scaffold processes.

Keywords

Hydroxyapatite-gelatin; Siloxane; Nanocomposite; Scaffold; Bone repair

Introduction

Critical size defect in bone represents a challenging problem and may require multiple-phase surgery to achieve adequate reparation and function. Autografts have achieved various degrees of success in treating bone defects. However, the autograft is limited by the donor site morbidity, prolonged rehabilitation, increased risk of deep infection and restricted

Corresponding author: Ching-Chang Ko, DDS, MS, Ph.D., Department of Orthodontics, School of Dentistry, University of North Carolina, CB #7454, Chapel Hill, NC 27599, Tel: 1-919-966-7329, Fax: 1-919-843-8497, koc@dentistry.unc.edu.

availability. Allografts might cause potential risks of transmitted diseases such as HIV or contamination [1, 2]. Thus, the development of synthetic biomaterials for alloplastic grafts is in high demand.

Hydroxyapatite (HAp) is a calcium-containing biomaterial composed of chemical elements similar to the mineral components in natural bone. The HAp possesses excellent properties that are required for bone grafts such as great stiffness, biocompatibility, cell affinity, and osteoconductivity [3–6]. There are two methods for HAp synthesis: sintering (high temperature) and precipitation (lower temperature). Because of lower surface activity, scaffolding of HAp requires a stereo lithographic process followed by high temperature (> 1250 C) sintering, a procedure limiting its clinical applicability. Calcium phosphate cement (CPC) involves dissolution of amorphous calcium phosphate and phase transformation to stabilized HAp precipitation. During the dissolution phase, CPC does not exhibit sufficient plasticity to form a controllable porous scaffold although blending with porogens (e.g., salt particles [7, 8] and paraffin microspheres [9, 10]) was reported. Alternatives have used calcium-alumina and magnesium-phosphate for 3D scaffolding [11, 12].

Hydroxyapatite-gelatin (HAp-Gel) system was developed by Chang et al. in 2003 [13] and it has been proven with chemical binding between hydroxyapatite and gelatin molecule, which mimics natural bone microstructure. The hydroxyapatite formed nanocrystal clusters within gelatinous particulates in a colloid slurry at 38 C. Various attempts have been made to cross-link HAp-Gel slurry particles after dehydration and solidification [14, 15]. Among these, siloxane cross-linker [16, 17] has been found to provide biocompatibility as biodegradable scaffold for bone regeneration, and thus has attracted lots of attention recently. A sol-gel process has been utilized by Ren et al. to synthesize porous gelatin-siloxane scaffolds for bone tissue engineering [18, 19]. The biodegradable gelatin and the bioactive inorganic components such as silanol group and calcium ions contribute to osteoconductivity. A solution process mixing aminosilane, bis[3-(trimethoxysilyl)propyl]-ethylenediamine (enTMOS) - a siloxane cross-linker, with HAp-Gel slurry combined with the salt leaching technique has also been utilized for hydroxyapatite-gelatin modified siloxane (GEMOSIL) scaffolding [20, 21]. Although the pore morphology of scaffolds was well controlled, the resultant scaffold was too brittle and contained inherent cracks. The solution process also took too long time to dehydrate because of excessive water. The contact angle measurements (data not shown here) also indicate that the freeze-dried HAp-Gel powders possess specific surface energy and reactivity in the ambient environment than the sintered hydroxyapatite powder. This discovery raises the question whether such high reactivity could render a powder process with robust formability to allow direct scaffolding at room temperature.

In the present study, we synthesized a GEMOSIL porous scaffold derived from a formable paste by a new powder process consisting of coating, kneading and hardening. The results showed that the gelatin content of HAp-Gel powder requires only minimal addition of buffer solution, yielding adhesion among the particles. When incorporating enTMOS coating, hydrogen bonding further enhanced the paste formability and finally HAp-Gel nanocrystals were interwoven inside the aminosilica matrix after hardening. The new powder process also allows the incorporation of TiO_2 to further improve osteoconductivity and bone formation. We hypothesized that the amount of aminosilane determines the formability of the paste and the strength of the final composite, and the presence of TiO_2 promotes osteogenic response *in vitro* and *in vivo*. Therefore, the objective of the present study is to investigate the effect of the enTMOS cross-linker on physical, mechanical, and surface chemical properties of the nanocomposites. Cell viability and animal test for GEMOSIL with/without TiO_2 addition were also studied.

Materials and Methods

Materials

The stock slurry of hydroxyapatite-gelatin (HAp-Gel) was prepared by the simultaneous titration method using peristaltic pumps (Masterflex, Cole-Parmer, USA), and a pH controller (Bukert 8280 H, Germany) [13]. Briefly, a double jacket beaker served as the reaction vessel. The temperature of the water bath was digitally controlled to within 0.1 °C. The amount of $Ca(OH)_2$ and H_3PO_4 was calculated to make 10 g of HAp. A homogeneous suspension that included $Ca(OH)_2$ dispersed in 1.2 L of an aqueous H_3PO_4 solution with a measured amount of gelatin (Type A : From porcine skin, Sigma-Aldrich, St. Louis, MO, USA) was gradually added to the reaction vessel through peristaltic pumps. After the coprecipitation reaction, the total volume was adjusted as 2.6 L. The temperature and pH of reaction solution in the vessel was maintained at 38 °C and 8.0, respectively. The amount of gelatin in H_3PO_4 aqueous solution was 5 g. The resulting slurries will be centrifuged at 5000 rpm under 4 °C for 30 minutes to remove excess water. The condensed HAp-Gel will be freeze dried at −80 °C overnight followed by lyophilization until dry, followed by grinding into fine particles. Bis[3-(trimethoxysilyl)propyl]ethylenediamine (enTMOS) was purchased from Gelest, Inc (Morrisville, PA, USA). Phosphate buffered saline (PH = 7.4) was obtained from Sigma-Aldrich Co. and TiO_2 (Evonik Aeroxide® P25) powder was supplied by Evonik Degussa Co. (Parsippany, NJ, USA) and used without further treatment.

Sample preparation and conditions

A 400 mg of HAp-Gel powder was transferred into a mortar and grinded into fine powder. The predetermined amount of enTMOS was added according to Table 1 and the mixture was continuously blended for another 3 minutes to form GEMOSIL powder. This GEMOSIL powder mixture appeared uniformly yellow color at this step and later was used for TEM measurement. To convert the mixture into GEMOSIL paste, 640 μL of phosphate buffer saline (PBS, 1X) was added to the GEMOSIL powder. After mixing for 2 minutes, another 160 μL of PBS was added into mixture followed by kneading for 2 minutes until the sample showed plasticity. At this state, GEMOSIL appeared as paste and was pressed with a mold to create round shape disc samples and cylindrical shape samples. All samples were solidified within an hour. The amount of enTMOS (95% concentration) used was 48, 96 and 144 μL, equivalent to 10.6, 19.2, 26.3 weight percentage. Sample notations were coded as GEMOSIL-11, GEMOSIL-19 and GEMOSIL-26 respectively, based on the enTMOS content (Table 1). The samples without enTMOS were also made for comparison (coded as HAp-Gel-PBS). For samples that contained TiO_2, the same procedure was followed except that a 38 mg of P25 powder was added prior to the mixing with enTMOS; and notation was coded as GEMOSIL-19-P25. All five groups of samples were used in the following experiments except for cell culture testing.

Mechanical testing

The mechanical testing consisted of compressive and Vickers hardness tests. After drying the samples under ambient environment for 5 days, the cylindrical shape samples with a 1 : 2 ratio of diameter (3.5 mm) to length (7.0 mm) were prepared for compressive test. The round disc samples for hardness testing were polished with the sand paper of grid sizes 600 and 1200 before measurement. Compressive testing was performed on an Instron 4204 (Canton, MA, USA) compression tester with a testing rate of 0.5 mm/min. Testworks 4 software (MTS. Inc) was used to analyze the data and the compressive strength was determined from the maximum strength value on the stress-strain curve. The hardness value was measured by Buehler MicrometII (Lake Bluff, IL, USA) Vickers hardness tester using 50 g constant load at a loading time of 15 sec. The measurement was performed every 24 hours in the period of 168 hours (7 days). The testing results were analyzed by one-way

ANOVA and followed by Tukey HDS comparison among the material groups. IBM SPSS statistics 19 (SPSS Inc., Chicago, IL, US) was used for all statistical analysis.

Contact angle testing

The disk samples were dried under ambient environment for 5 days. The contact angle was measured using conventional contact angle instrument (200-F1, Rame-Hart Instrument Co., Succasunna, NJ, US) by placing a disc shape sample onto a platform underneath a water syringe and in front of a CCD camera. DropImage 2.4.04 software (Rame-Hart Instrument Co.) was used for measurements and the images of the droplet were taken when each water droplet stabilized and remained symmetrical on the disc surface. The contact angle was measured from the digital photo with image analysis software. Each measurement was repeated two times.

Thermogravimetric analyzer (TGA) testing

GEMOSIL samples of various amounts of enTMOS (Table 1) were synthesized, cured in the air, and grinded into powders. Each 10 mg of powder was placed on a platinum sample holder, and the sample holder was loaded inside the Q-500 thermogravimetric analyzer (TA Instrument, New Castle, DE, US). Q Series 2.5 software (TA Instrument) was used for data analysis. The TGA test was performed from 30 C to 800 C with a heating rate of 5° C/min. Weight changes were recorded versus temperature. The weight percentage of individual components (H_2O, gelatin, HAp, Silica) in each sample was estimated from the TGA data.

Transmission electron microscopy (TEM)

Transmission electron microscopy (TEM) was performed on a JEOL 2010F using an accelerated voltage of 200 kV. To prepare samples suitable for TEM observation, sample was prepared by dispersing enTMOS-treated GEMOSIL powder in methanol and sonicating for 20 minutes. Then, formvar/carbon-coated TEM grids were immersed in the mixture solution followed by drying at room temperature.

Cell culture testing

The GEMOSIL-19 was chosen, based on the result of mechanical tests, to further study its influence on preosteoblast proliferation and differentiation. Three experimental groups of materials were investigated, including GEMOSIL-19, GEMOSIL-19-P25, and dishes as received without coating (control). Preosteoblasts, MC3T3-E1, were cultured in 96-well plates (Falcon, Becton, Dickinson Labware, Frankin Lakes, NJ, USA) in which all wells were coated with the specified material. Cells were seeded at a density of 1×10^4 per milliliter using αMEM medium supplemented with 10% of FBS and 1% penicillin/streptomycin under 37 C, 5% CO_2 atmosphere. Cellular metabolic activity was determined with MTS colorimetric assay at day 1, 4, 7, 10 and 13 according to the manufacturer's instructions (CellTiter96; Promega, Madison, WI, USA). Briefly, 20 μL of MTS reagent was added to the cells in 96 well plates at the end of the designed cultivation period and incubated for 1 hour at 37 C. Colored formazan products were quantified by measuring absorbance at 490 nm (plate reader). The average background (medium plus MTS without cells) was subtracted from the absorbance values of experimental groups for normalization purposes. The resultant optical densities were quantified to assess cell proliferation for each group. Three samples were tested with triplicate at each time point for each group.

Assessment for cell differentiation on the material was performed using the Alizarin Red as a calcium mineralization stain. Three groups including GEMOSIL-19 coated, GEMOSIL-19-P25 coated and uncoated (as received) 35 mm Petri dishes were used for differentiation studies. The same groups without cell seeding were used as control for

quantification analysis. A total of 3.2×10^5 MC3T3-E1 cells were seeded onto the dish and pre-cultured for 3 days to reach confluence using the above same growth medium and conditions. After three days, the differentiation medium was supplemented with 10 mM B-glycerophosphate and 0.2 mM ascorbic acid and cultured for 14 days. Visual indication for calcification was achieved by Alizarin Red (Acros Organics, Geel, Belgium) staining using manufacturer's protocol [22]. The quantification results of mineralization characteristics were derived from color differences (δ) by CIELAB method. Optical color measurement, CIELAB (the Commission Internationale de I'Eclairage) tristimulus values, was based on the principle of light transmission which is wavelength-dependent. Given an externally applied illuminating light to the stain, the detectable color spectrum was used as signals to differentiate and analyze the degree of mineralization. The dish colors of the digital images were converted to CIELAB tristimulus values for each image pixel. The tristimulus values of ten evenly distributed points from each dish were calculated relative to the Commission Internationale de I'Eclairage (CIE). The characteristic values and standard deviations for L, a*, and b* were calculated using the Photoshop software (Adobe System Inc., CA). For each material group, a formula to calculate the mineralization's characteristics was a color difference between the with and the without cell dishes,

$\delta=((L-L_o)^2+(a^*-a^*_o)^2+(b^*-b^*_o)^2)^{1/2}$ where (L, a*, b*) and (L_o, a^*_o, b^*_o) were tristimulus values for the having cell and non-cell dish, respectively. The mean δ were compared among three groups using one way ANOVA and Tukey-Kramer's HSD. IBM SPSS Statistics 19 (SPSS Inc., Chicago, IL, US) was used for all statistical analysis.

Bone regeneration in rat calvarium defects

GEMOSIL-19 and GEMOSIL-19-P25 porous scaffolds with bases were implanted in 8mm critical-size defects (CSD) in rat calvaria. The craniofacial defect consisted of an 8mm-diameter calvaria critical-size defect, which has previously been described [23]. Briefly, 11- to 13-week-old Sprague-Dawley rats (Charles River, Wilmington, MA) were anesthetized and an 8-mm-diameter defect was created on the calvaria bone using a dental trephine drill. Three rats were used for each material. Animals were euthanized either at 8 weeks after surgery, calvaria specimens were retrieved and fixed in 10% formalin for 7 days and then transferred to isopropanol 70% for non-decalcified sectioning. The tissue sections were stained with Stevenel's Blue and Van Gieson to assess the formation of newly formed bone (NFB) tissue. All procedures were compliant with the animal care regulation at University of North Carolina - Chapel Hill (IACUC09-270.0-B).

Results

The formable GEMOSIL paste is illustrated in Fig.1a. This plastic property would be ideal for making complicated scaffold geometries as well as injectable scaffolding (Fig.1b). The final composites appear white or yellowish depending on the amount of enTMOS and TiO_2 additive. The compressive strength (Fig.2) varies significantly with the amount of enTMOS ($p < 0.01$). The strength increases as enTMOS increases and reaches a maximum when enTMOS amount is about 10.6 wt% ~ 19.2 wt% without apparent difference in the compressive strength according to Tukey HDS test. However, adding TiO_2 lowered the strength by 20% when compared to the sample without it.

One way ANOVA showed that Vickers hardness (HV) (Fig.3) of the composite increased significantly with enTMOS ($p < 0.01$). The value of HV reached the maximum when sample contained 26.3 wt% of enTMOS. Compared to the aminosilane treated samples, the untreated samples were more susceptible to fracture and had lower hardness. By adding TiO_2, the surface hardness increased 5% compared to the sample without TiO_2 due to the high modulus of TiO_2 particles. The hardness value increased over time and reached a

maximum after 120 hours, which indicates that the complete hardening time would be 5 days.

According to TGA measurements, the absorbed water inside the GEMOSIL solid could not be removed completely until 200 C [24] (Fig.4). The data revealed that slightly more water was trapped in GEMOSIL than in HAp-Gel-PBS sample. The HAp-Gel-PBS samples showed three distinct weight drops, contributing to the degradation of gelatin [25]. The GEMOSIL sample showed similar TGA pattern when compared to HAp-Gel-PBS sample, except for the final degradation region between 400–C 500 C, which was attributed to the degradation of aminosilica. The weight reduction increased as the amount of aminosilica increased; this was due to the decomposition of hydrocarbon on aminosilica molecules. The amount of aminosilica after setting was derived by TGA results and Fig.5 compares the theoretical weight percentage of aminosilica to that of the actual content in the final composite. The discrepancy between the theoretical and actual contents suggests that there were aminosilica remained in nanocomposites at 800 C and the residual component increased as the aminosilica amount increased. The remaining weight was contributed by silica and HAp phases after 800 C.

The TEM images were obtained for GEMOSIL-11 (Fig.6a) and GEMOSIL-19 (Fig.6b) samples after enTMOS treatment. The needle shape structures represent the typical HAp-Gel nanocrystals derived from the precipitation process [13]. The TEM images also confirmed the integrity of HAp-Gel nanocrystals where the needle shape crystals are embedded inside the matrix without damage. This result indicates the new dry grinding process used to apply enTMOS coating preserves the structure of HAp-Gel nanocrystals. However, the GEMOSIL-11 sample shows more distinct needle shape nanocrystals, which might be due to the different amount of enTMOS coating.

There is no obvious difference in the contact angle measurements between HAp-Gel-PBS and GEMOSIL samples (Fig.7). The enTMOS did not change the hydrophilic properties of the composites. However, the addition of the TiO_2 increased the contact angle by 10 degrees, indicating a decrease of hydrophilicity on the material surface, which might affect cell adhesion [26]. The cell growth (proliferation) curves showed no differences over time between the GEMOSIL-19-P25 dish and the positive control (Fig.8). The cell growth on the GEMOSIL-19 had the lowest growing rate among three groups. However, Alizarin red stain showed the equal ability of preosteoblasts to mineralize at day 14 on both the GEMOSIL and the GEMOSIL-19-P25 superior to the control (Fig.9).

For the calvarium defect study, both GEMOSIL-19 and GEMOSIL-19-P25 revealed new bone formation 8weeks after implantation. GEMOSIL-19-P25 (red arrows in Fig.10b) had more areas and thicker islands (50–300 μm diameter) of bone formation within the pore space than GEMOSIL-19 (red arrows in Fig.10a), suggesting that titania additives could increase *in vivo* bone ingrowth on the HAp-Gel biomaterial surfaces. GEMOSIL-19 resulted in thin (15–35 μm) and network-like bone nodules.

Discussion

The cohesive strength of the powder depends upon interparticular interactions such as electrostatic forces, van der Waals force, hydrogen bonding, and steric hindrance. Gelatin is known to possess polyampholytic and polyelectrolytic properties due to its intrinsic protein composition [27, 28]. The carboxylic and amino groups of gelatin may absorb water molecular and cause swelling [29]. The swelling of gelatin maintains water content and hydrogen bonding within GEMOSIL paste providing lubrication for molecular movement, which contributes to materials' formability. Simultaneously, these functional groups also

form hydrogen bonds with silanol group of aminosilica [21, 30] to provide additional cohesive strength of formability. The siloxane also has been shown to form hydrogen bonding hydroxyapatite [31], which provides additional cohesive strength. This synergetic effect between biological and mineral components contributed to the formable plasticity of the GEMOSIL paste. The hydrogen bonding provided weak bonding force and allowed short distance sliding between the HAp-Gel particles, which resulted in formable properties [32, 33]. The paste could be packed into a syringe and extruded without creeping overtime, and the final porous scaffolding (Fig.1b) suggests that the present processes are capable of achieving acceptable moldable property, which would be suitable for complex geometry scaffolding.

The residual water in GEMOSIL samples was more than that of HAp-Gel-PBS sample, which indicates the stronger hydrogen bonding within GEMOSIL nanocomposites causing excessive water absorption [34]. This strong hydrogen bonding is critical to the plasticity and processibility of the material. The gelatin degradation temperature was 420 C in HAp-Gel and shifted to higher temperature when enTMOS content increased, which proves the presence of chemical bonding between HAp-Gel and enTMOS. It is interesting to note on Fig.5 that the percentage of the decomposed enTMOS from the TGA calculation decreased with the increase of enTMOS coating in the composite, which indicates the alkyl side groups did not decompose completely. This result may be due to that the alkyl side groups inside a highly cross-linked silica phase did not fully react with oxygen. The TEM images of GEMOSIL-11 (Fig.6a) and GEMOSIL-19 (Fig.6b) appeared to confirm that the enTMOS layer preserved the structure of HAp-Gel nanocrystals from damage during the coating process. This coating process by dry grinding method was also effective as evidenced that 8~16 wt% enTMOS was quantified via TGA data.

Besides the formability, siloxane also provided the effective cross-linkage for HAp-Gel within nanocomposites. Siloxane has been considered as potentially effective cross-linking agent due to their interaction with some poly-amino acids and proteins via both electrostatic forces and hydrogen bondings [35, 36]. Gelatin consists of various amounts of aminoacids, including glycine, proline and hydroxyproline [37]. It would be expected that these amino acid contained in its structure could form the hydrogen bonding with silanol groups. In our previous FTIR study [21], the bands at 1647 cm^{-1} in the spectra corresponded to the gelatin's amide I band due to CO stretching. The results showed a red shift in amide I band to the lower wavenumber indicating the hydrogen bonding of the CO in gelatin to the silanol hydrogen [38]. These interactions could be used to induce physical cross-linkage [39, 40]. The formation of the continuous aminosilica phases within GEMOSIL nanocomposites relies on the cross-linkage of the enTMOS. This sol-gel reaction consists of hydrolysis and condensation reactions. First, enTMOS reacted with water and replaced methoxy (Me) group by hydroxyl (OH) group with methanol release attributed to hydrolysis reaction (Eq. 1). Then, the two hydrolyzed molecules can link together in a condensation reaction to form a siloxane bond (Eq.2).

$$Si(OMe)_4 + 4\,H_2O \rightarrow Si(OH)_4 + 4\,MeOH \quad (1)$$

$$Si(OH)_4 \rightarrow SiO_2 + 2H_2O \quad (2)$$

The compression data confirmed our hypothesis that there exists an optimal range of enTMOS for GEMOSIL nanocomposites. Both the high and low amount of enTMOS reduces the strength of the composite. In theory, HAp-Gel particles do not form strong aggregates when there are insufficient enTMOS binders. The HAp-Gel-PBS sample without enTMOS showed a low compressive strength. On the contrary, high amount of binder could

leave a thick, porous silica layers between the particles, which are prone to fracture. The redundant coating increases the amount of nanoporous, brittle glassy phases between HAp-Gel particles and, therefore, increase the chance for crack nucleation and propagation, which decrease the mechanical properties of composite materials [41, 42]. The increased volume of brittle silica phase due to thicker coating among HAp-Gel particles were also confirmed by TGA results. The enTMOS coating provides strong intermolecular force for the nanocomposites and hence increases the surface hardness. The hardness test was performed to measure the resistance to permanent shape change when a force applied to assess the intermolecular bonds within composite materials [43]. The data shows that hardness increases with the amount of enTMOS. This coupling agent is primarily used to enhance the bonding among particles and between different phases within composite materials. The amount of coupling agent has a great influence on the micro structure and strength of the composites [44, 45]. The hardness value also increased throughout the aging process (up to 120 hours), which is attributed to the complete condensation reaction within the gel that further enhances the network structure and mechanical properties of the nanocomposites.

From these remarks, a model (coating, kneading and hardening) can be proposed to explain the setting mechanism, as illustrated in Fig.11. **Coating stage:** The coating layer of enTMOS was proven by detecting the chemical bonding formation between different phases of compounds [21]. At this point, hydrogen bonds and Si-O-P bonding began to form at the interface between the thin enTMOS coating and HAp-Gel particles. In this stage, the particles did not aggregate together because there was not enough water to induce sol-gel reactions. **Kneading stage:** After adding PBS and performing kneading process, water molecules filled in the gaps between enTMOS and HAp-Gel, forming hydrogen bonds within/between phases. In the same time, the excessive water also induced the hydrolysis and condensation reactions of enTMOS, making paste less formable over time. The processing window (working time) for formable plasticity properties was around five minutes. **Hardening stage:** At the end of working time, hardness increased due to the formation of silica phase. This formation of the solid matrix was the result of the condensation reaction. The silica phase is believed to be nanoporous structure that contained water and held the structure together. During hardening, condensation reaction continued to occur and further strengthen the silica phase, which increased the overall strength of the final sol-gel materials [46]. Further drying eliminated the water inside the pore structures, condensed the silica phases into rigid monoliths. The present dry powder approach shortened the processing time for samples and scaffold fabrications. The drying process lasted for twelve hours until the weight stopped changing, which was relatively short compared to the previous solution method [21]. In summary, at the completion of sol-gel reaction, enTMOS served as binder and matrix for the HAp-Gel particles and formed rigid nanocomposites.

TiO_2 appeared to enhance osteogenesis by affecting both proliferation and differentiation of preosteoblasts. The color analysis was directed towards performing stain intensity and wave analysis of photon signals generated by the transmission light, quantifying the signals and correlating the sources with microstructural parameters, e.g., sizes and numbers of mineral nodules. The CIELAB color system provided an orthogonal, three-dimensional space in which color is defined by three coordinates: lightness (L), red-green (a*), and yellow-blue (b*). The uniform color space provided by the CIELAB system had the property that a perceived difference, defined as δ, between colors is quantitatively the same in all its areas [47]. It appeared the mineralization (ability of biomaterials to promote cell differentiation) of three groups was distinguishable using quantitative δ values

The *in vivo* data further confirmed the *in vitro* outcomes. Our data were consistent with those of previous studies suggesting that TiO_2 could enhance the biocompatibility of

bioceramics because TiO_2 increased calcium ion interactions, promoted protein and cell adhesion, and differentiation and mineralization of preosteoblasts [48, 49]. Hydrophobic adsorption has been considered as one of the most important mechanisms for protein adsorption. Several studies have shown the similar results that the quantity of proteins adsorbed is higher on the more hydrophobic surface [50, 51]. Besides stable adsorption of protein, the protein must retain its configuration to react with receptors for cell attachment. Topoglidis and coworkers have found stable immobilisation of various proteins on TiO_2 film with a high binding stability and no detectable denaturation [52]. Also, the molecular dynamic simulation showed denaturation of BMP-2 induced by adsorption was not observed at the initial stage of adsorption [53]. These proteins can facilitate the attachment of various cells such as osteoblasts that can stimulate bone repairs. Thus, relative hydrophobic GEMOSIL-19-P25 suggested that there might be more proteins absorbed onto the material surfaces. Sequentially, more MC3T3-E1 cells adhered to the material surface and facilitate cellular proliferation and differentiation. Histological data proved that newly formed bone was abundant and seamlessly adhered to the GEMOSIL-19-P25 surface more than GEMOSIL-19, suggesting that TiO_2 might prepone host marrow stromal cells to osteogenic path. The formation of the harvasian system suggested that an intramembranous bone formation may be associated with the TiO_2 additives. Future investigation assessing gene expression may provide necessary information for its biological mechanism. The compressive results implied that TiO_2 might decrease efficacy of enTMOS cross-linker. It is, however, a trade off by using TiO_2 to promote biological properties of the GEMOSIL scaffold.

Conclusion

This study reports a new method of scaffolding made of hydroxyapatite-gelatin and aminosilane nanocomposites. The moldable properties of GEMOSIL owing to inherit gelatin's and aminosilane's bonding interaction would be favored for complicated scaffolding. In particular, the aminosilane binder affects final mechanical strength of the scaffold in a non-linear mater, with optimal concentration being 11–19 wt%. The process also allowed the addition of TiO_2 to enhance osteoconductivity of MC3T3-E1 preosteoblasts and *in vivo* bone formation. In summary, the new GEMOSIL nanocomposites could provide opportunities of easy handling, sturdy materials, and direct scaffolding for potential tissue engineering applications.

Acknowledgments

This work was supported, in part, by NIH/NIDCR K08DE018695, NC Biotech and American Association for Orthodontist Foundation. Although CC Ko is the co-founder of Ironwood Materials Science Inc., this study was not supported by any companies.

References

1. Hou CH, Yang RS, Hou SM. Hospital-based allogenic bone bank-10-year experience. J Hosp Infect. 2005; 59:41. [PubMed: 15571852]
2. Nishida J, Shimarnura T. Methods of reconstruction for bone defect after tumor excision: A review of alternatives. Med Sci Monitor. 2008; 14:RA107.
3. Bucholz RW, Carlton A, Holmes RE. Hydroxyapatite and Tricalcium Phosphate Bone-Graft Substitutes. Orthop Clin North Am. 1987; 18:323. [PubMed: 3561978]
4. Ishihara K, Arai H, Nakabayashi N, Morita S, Furuya K. Adhesive Bone-Cement Containing Hydroxyapatite Particle as Bone Compatible Filler. J Biomed Mater Res. 1992; 26:937. [PubMed: 1607374]

5. Radin SR, Ducheyne P. Effect of Bioactive Ceramic Composition and Structure on in-Vitro Behavior .3. Porous Versus Dense Ceramics. J Biomed Mater Res. 1994; 28:1303. [PubMed: 7829560]
6. Narasaraju TSB, Phebe DE. Some physico-chemical aspects of hydroxylapatite. J Mater Sci. 1996; 31:1.
7. Tas AC. Preparation of porous apatite granules from calcium phosphate cement. J Mater Sci-Mater Med. 2008; 19:2231. [PubMed: 18049869]
8. Hesaraki S, Zamanian A, Moztarzadeh F. The influence of the acidic component of the gas-foaming porogen used in preparing an injectable porous calcium phosphate cement on its properties: Acetic acid versus citric acid. J Biomed Mater Res Part B. 2008; 86B:208.
9. Yu NYC, Schindeler A, Little DG, Ruys AJ. Biodegradable Poly(alpha-hydroxy acid) Polymer Scaffolds for Bone Tissue Engineering. J Biomed Mater Res Part B. 93B:285.
10. Silva TSN, Primo BT, Silva AN, Machado DC, Viezzer C, Santos LA. Use of calcium phosphate cement scaffolds for bone tissue engineering: in vitro study. Acta Cir Bras. 2011; 26:7. [PubMed: 21271197]
11. Maier AK, Dezmirean L, Will J, Greil P. Three-dimensional printing of flash-setting calcium aluminate cement. J Mater Sci. 46:2947.
12. Klammert U, Vorndran E, Reuther T, Muller FA, Zorn K, Gbureck U. Low temperature fabrication of magnesium phosphate cement scaffolds by 3D powder printing. J Mater Sci-Mater Med. 21:2947. [PubMed: 20740307]
13. Chang MC, Ko CC, Douglas WH. Preparation of hydroxyapatite-gelatin nanocomposite. Biomaterials. 2003; 24:2853. [PubMed: 12742723]
14. Chang MC, Ko CC, Douglas WH. Modification of hydroxyapatite/gelatin composite by polyvinylalcohol. J Mater Sci. 2005; 40:2723.
15. Chang MC, Douglas WH. Cross-linkage of hydroxyapatite/gelatin nanocomposite using imide-based zero-length cross-linker. J Mater Sci-Mater Med. 2007; 18:2045. [PubMed: 17558474]
16. Dunn B, Miller JM, Dave BC, Valentine JS, Zink JI. Strategies for encapsulating biomolecules in sol-gel matrices. Acta Mater. 1998; 46:737.
17. Coradin T, Bah S, Livage J. Gelatine/silicate interactions: from nanoparticles to composite gels. Colloid Surf B-Biointerfaces. 2004; 35:53.
18. Ren L, Tsuru K, Hayakawa S, Osaka A. Novel approach to fabricate porous gelatin-siloxane hybrids for bone tissue engineering. Biomaterials. 2002; 23:4765. [PubMed: 12361615]
19. Ren L, Tsuru K, Hayakawa S, Osaka A. In vitro evaluation of osteoblast response to sol-gel derived gelatin-siloxane hybrids. J Sol-Gel Sci Technol. 2003; 26:1137.
20. Ko, CC.; Luo, TJM.; Chi, L.; Ma, A. Advances in Bioceramics and Porous Ceramics. Vol. 29. Westerville: Amer Ceramic Soc; 2009. Hydroxyapatite/Gemosil Nanocomposite; p. 123
21. Luo TJM, Ko CC, Chiu CK, Llyod J, Huh U. Aminosilane as an effective binder for hydroxyapatite-gelatin nanocomposites. J Sol-Gel Sci Technol. 2010; 53:459.
22. Gregory CA, Gunn WG, Peister A, Prockop DJ. An Alizarin red-based assay of mineralization by adherent cells in culture: comparison with cetylpyridinium chloride extraction. Anal Biochem. 2004; 329:77. [PubMed: 15136169]
23. Ferreira, J. Engineering hydroxyapatite-gelatin nanocomposites with MAPC cells for calvarium bone regeneration. University of North Carolina; Chapel Hill: 2011. vol. Ph.D(in press)
24. Zholobenko V, Garforth A, Dwyer J. TGA-DTA study on calcination of zeolitic catalysts. Thermochim Acta. 1997; 294:39.
25. Word, AGCA. The science and technology of gelatin. London: Academic Press; 1977.
26. Horbett TA, Waldburger JJ, Ratner BD, Hoffman AS. Cell-Adhesion to a Series of Hydrophilic-Hydrophobic Copolymers Studied with a Spinning Disk Apparatus. J Biomed Mater Res. 1988; 22:383. [PubMed: 3397378]
27. Veis, A. The macromolecular chemistry of gelatin. New York: Academic Press; 1964.
28. Darder M, Ruiz AI, Aranda P, Van Damme H, Ruiz-Hitzky E. Bio-nanohybrids based on layered inorganic solids: Gelatin nanocomposites. Curr Nanosci. 2006; 2:231.

29. Ren L, Tsuru K, Hayakawa S, Osaka A. Synthesis and characterization of gelatin-siloxane hybrids derived through sol-gel procedure. J Sol-Gel Sci Technol. 2001; 21:115.
30. Coradin T, Durupthy O, Livage J. Interactions of amino-containing peptides with sodium silicate and colloidal silica: A biomimetic approach of silicification. Langmuir. 2002; 18:2331.
31. Dupraz AMP, deWijn JR, vanderMeer SAT, deGroot K. Characterization of silane-treated hydroxyapatite powders for use as filler in biodegradable composites. J Biomed Mater Res. 1996; 30:231. [PubMed: 9019488]
32. Laird DA. Bonding between polyacrylamide and clay mineral surfaces. Soil Sci. 1997; 162:826.
33. Lee SR, Park HM, Lim H, Kang TY, Li XC, Cho WJ, Ha CS. Microstructure, tensile properties, and biodegradability of aliphatic polyester/clay nanocomposites. Polymer. 2002; 43:2495.
34. Tang Y, Finlay JA, Kowalke GL, Meyer AE, Bright FV, Callow ME, Callow JA, Wendt DE, Detty MR. Hybrid xerogel films as novel coatings for antifouling and fouling release. Biofouling. 2005; 21:59. [PubMed: 16019392]
35. Coradin T, Livage J. Effect of some amino acids and peptides on silicic acid polymerization. Colloid Surf B-Biointerfaces. 2001; 21:329.
36. Coradin T, Coupe A, Livage J. Interactions of bovine serum albumin and lysozyme with sodium silicate solutions. Colloid Surf B-Biointerfaces. 2003; 29:189.
37. Segtnan VH, Isaksson T. Temperature, sample and time dependent structural characteristics of gelatine gels studied by near infrared spectroscopy. Food Hydrocolloids. 2004; 18:1.
38. Farhat IA, Orset S, Moreau P, Blanshard JMV. FTIR study of hydration phenomena in protein-sugar systems. J Colloid Interface Sci. 1998; 207:200. [PubMed: 9792763]
39. Fujitsu M, Hattori M, Tamura T. Effects of hydroxy compounds on gel formation of gelatin. Colloid Polym Sci. 1997; 275:67.
40. Wu J, Chiu SC, Pearce EM, Kwei TK. Effects of phenolic compounds on gelation behavior of gelatin gels. J Polym Sci Pol Chem. 2001; 39:224.
41. Baji A, Wong SC, Srivatsan TS, Njus GO, Mathur G. Processing methodologies for polycaprolactone-hydroxyapatite composites: A review. Mater Manuf Process. 2006; 21:211.
42. Causa F, Netti PA, Ambrosio L, Ciapetti G, Baldini N, Pagani S, Martini D, Giunti A. Poly-epsilon-caprolactone/hydroxyapatite composites for bone regeneration: in vitro characterization and human osteoblast response. J Biomed Mater Res Part A. 2006; 76A:151.
43. Thomas V, Dean DR, Jose MV, Mathew B, Chowdhury S, Vohra YK. Nanostructured biocomposite scaffolds based on collagen coelectrospun with nanohydroxyapatite. Biomacromolecules. 2007; 8:631. [PubMed: 17256900]
44. Schutte CL. Environmental Durability of Glass-Fiber Composites. Mater Sci Eng R-Rep. 1994; 13:265.
45. Kent MS, Smith GS, Baker SM, Nyitray A, Browning J, Moore G, Hua DW. The effect of a silane coupling agent on water adsorption at a metal/polymer interface studied by neutron reflectivity and angle-resolved X-ray photoelectron spectroscopy. J Mater Sci. 1996; 31:927.
46. Dumas J, Quinson JF, Bovier C, Baza S, Serughetti J. Correlations between Textural and Mechanical-Properties in Wet Silica-Gels. J Non-Cryst Solids. 1986; 82:220.
47. German R, Guzowski M, Wright D. The colour of gold-silver-copper alloys. Gold Bulletin. 1980; 13:113.
48. Ellingsen JE. A Study on the Mechanism of Protein Adsorption to Tio_2. Biomaterials. 1991; 12:593. [PubMed: 1663394]
49. Kitsugi T, Nakamura T, Oka M, Yan WQ, Goto T, Shibuya T, Kokubo T, Miyaji S. Bone bonding behavior of titanium and its alloys when coated with titanium oxide (TiO_2) and titanium silicate (Ti_5Si_3). J. Biomed. Mater. Res. 1996; 32:149.
50. Malmsten M. Formation of adsorbed protein layers. J Colloid Interface Sci. 1998; 207:186. [PubMed: 9792762]
51. Yoon JY, Park HY, Kim JH, Kim WS. Adsorption of BSA on highly carboxylated microspheres - Quantitative effects of surface functional groups and interaction forces. J Colloid Interface Sci. 1996; 177:613.

52. Topoglidis E, Cass AEG, O'Regan B, Durrant JR. Immobilisation and bioelectrochemistry of proteins on nanoporous TiO2 and ZnO films. J Electroanal Chem. 2001; 517:20.

53. Utesch T, Daminelli G, Mroginski MA. Molecular Dynamics Simulations of the Adsorption of Bone Morphogenetic Protein-2 on Surfaces with Medical Relevance. Langmuir. 27:13144. [PubMed: 21958113]

Fig. 1.
GEMOSIL paste for direct scaffolding. Formable GEMOSIL paste can be molded into a (a) cube by hand and injected to form a (b) porous scaffold

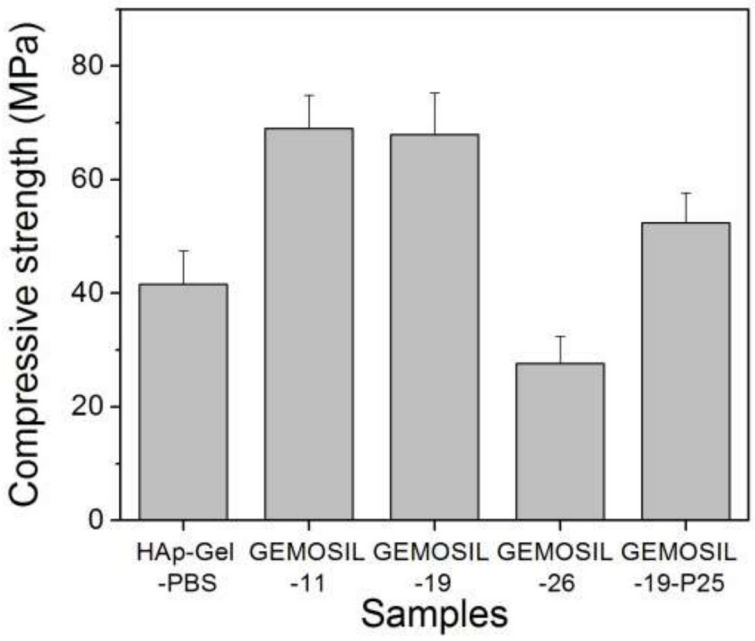

Fig. 2.

The compressive strength of GEMOSIL nanocomposites. The optimal compressive strengths of GEMOSIL nanocomposites are observed when enTMOS percentage is between 11 wt% and 19 wt%. Decrease of strength due to TiO_2 (GEMOSIL-19-P25) is not statistically significant ($p = 0.25$)

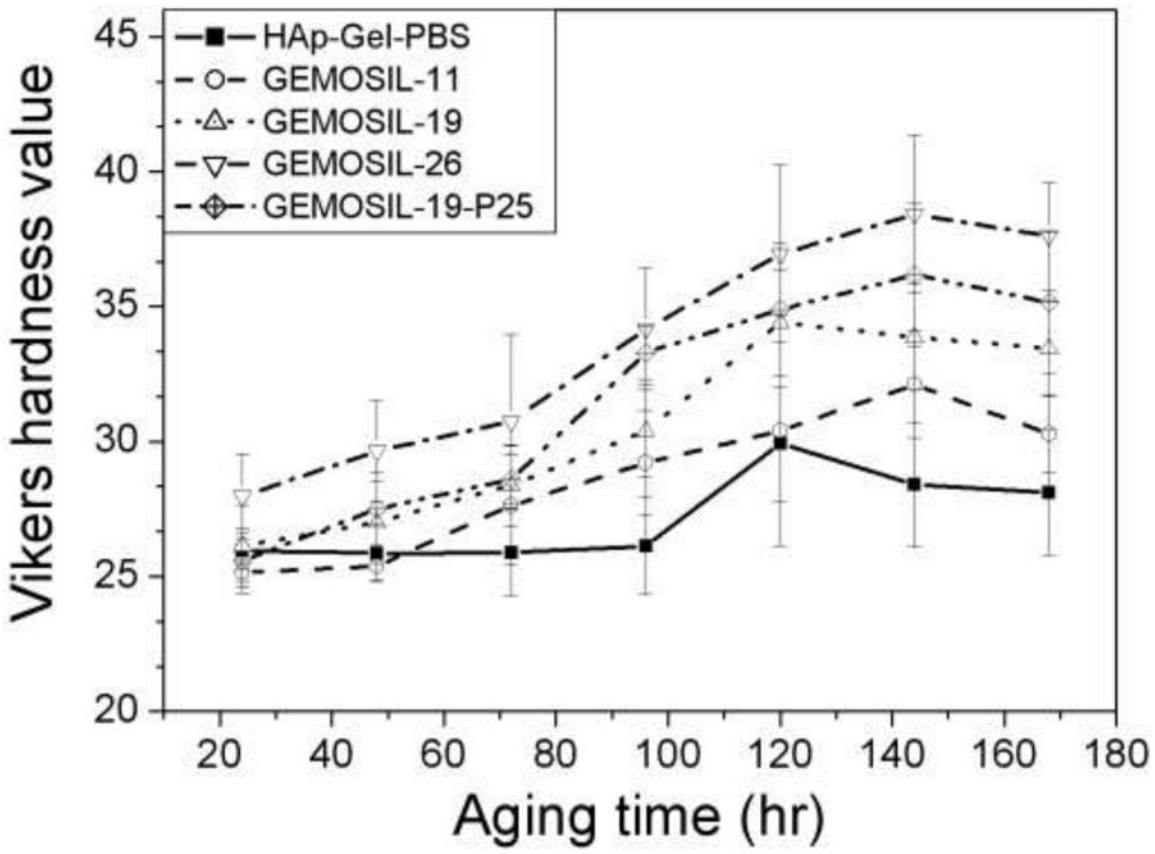

Fig. 3.

Vickers hardness (HV) of GEMOSIL nanocomposites. HV increases with the amount of enTMOS ($p < 0.01$) and the aging time. HV reaches the maximum when sample contains 26.3 wt% of enTMOS

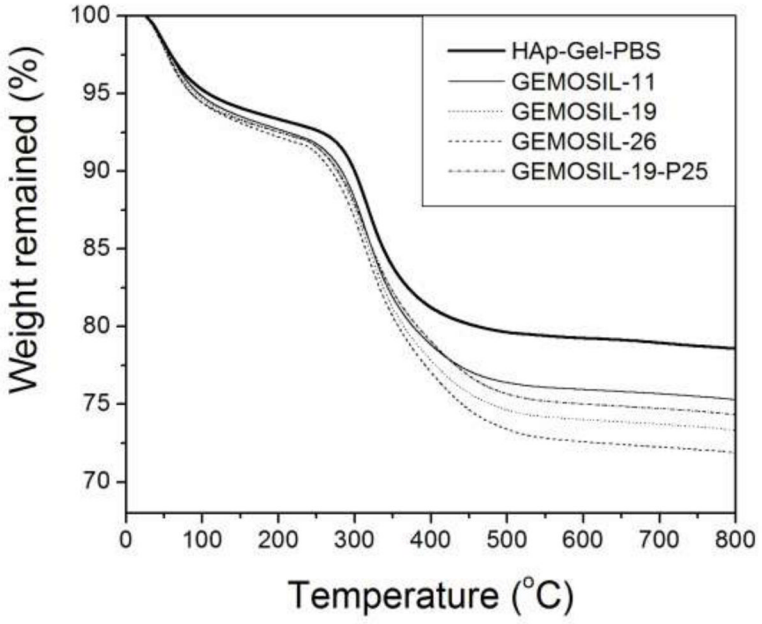

Fig. 4.
TGA analysis of GEMOSIL nanocomposites. Distinct weight drop patterns are attributed to the elimination of water, gelatin, and alkyl side groups

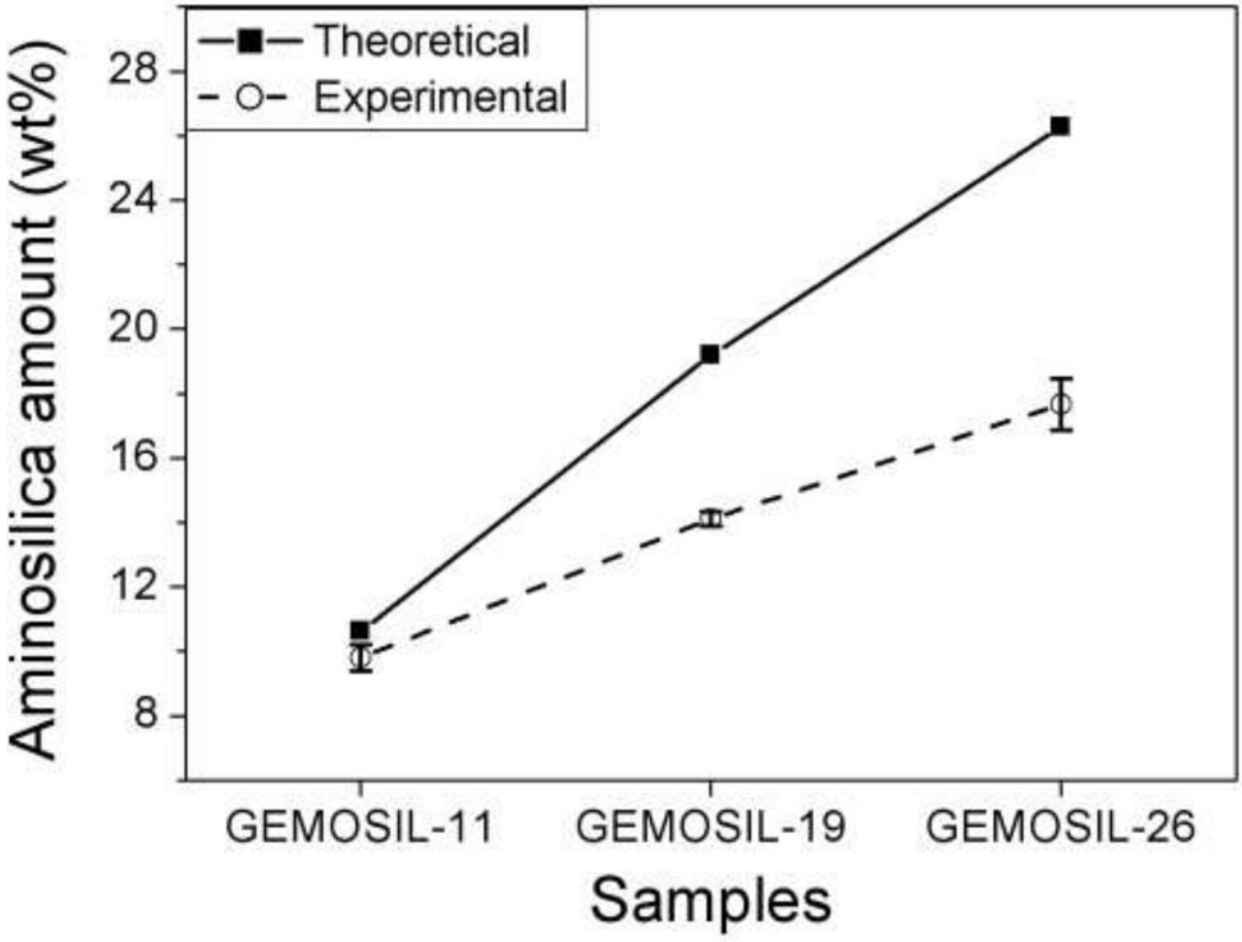

Fig. 5.
Theoretical predictions and experimentally measured weight percentages of aminosilica in GEMOSIL samples. The discrepancy between the two measures suggests that there exists residual aminosilica in the nanocomposites after 800 C treatment and residuals increase with aminosilica amount

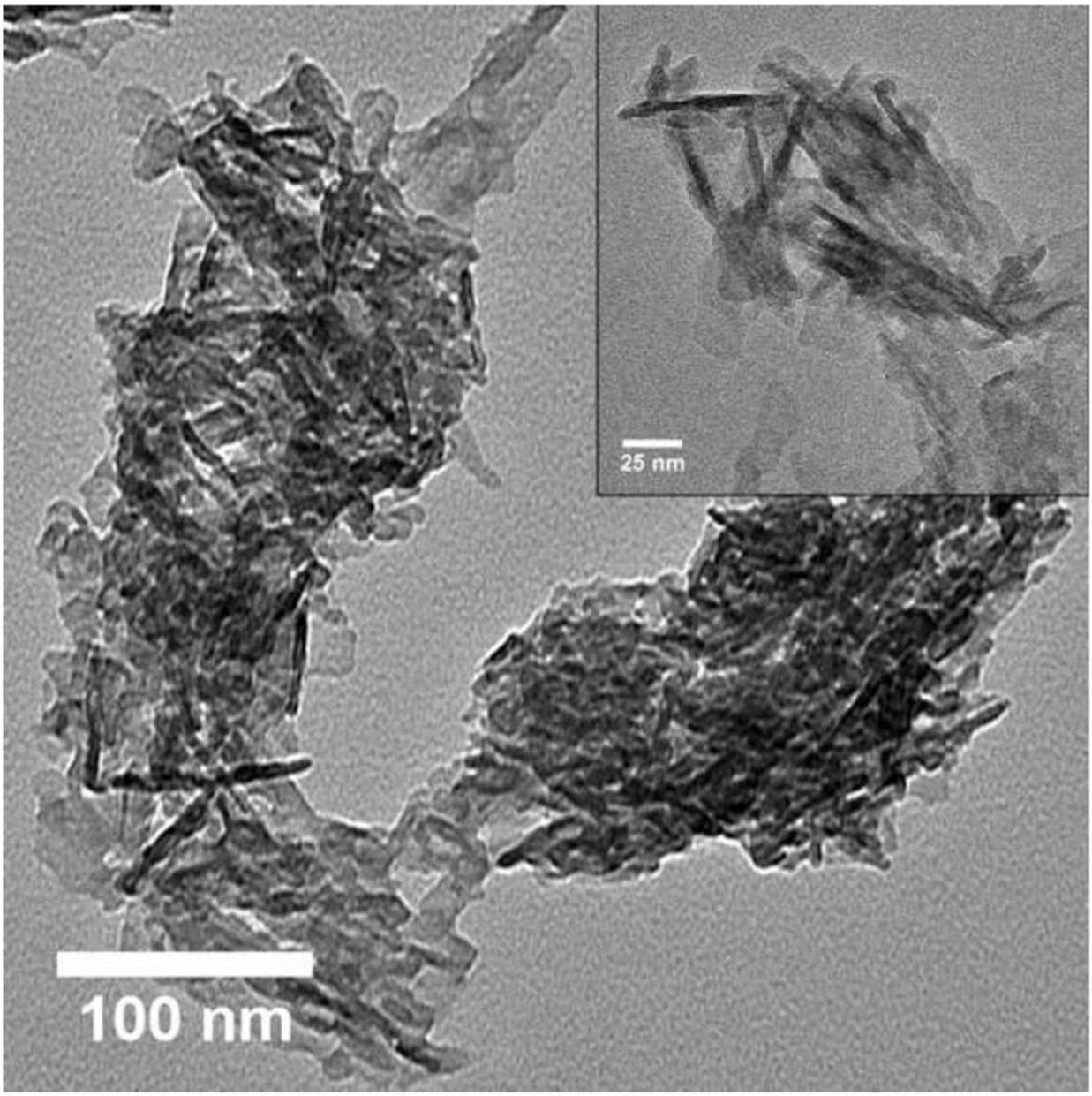

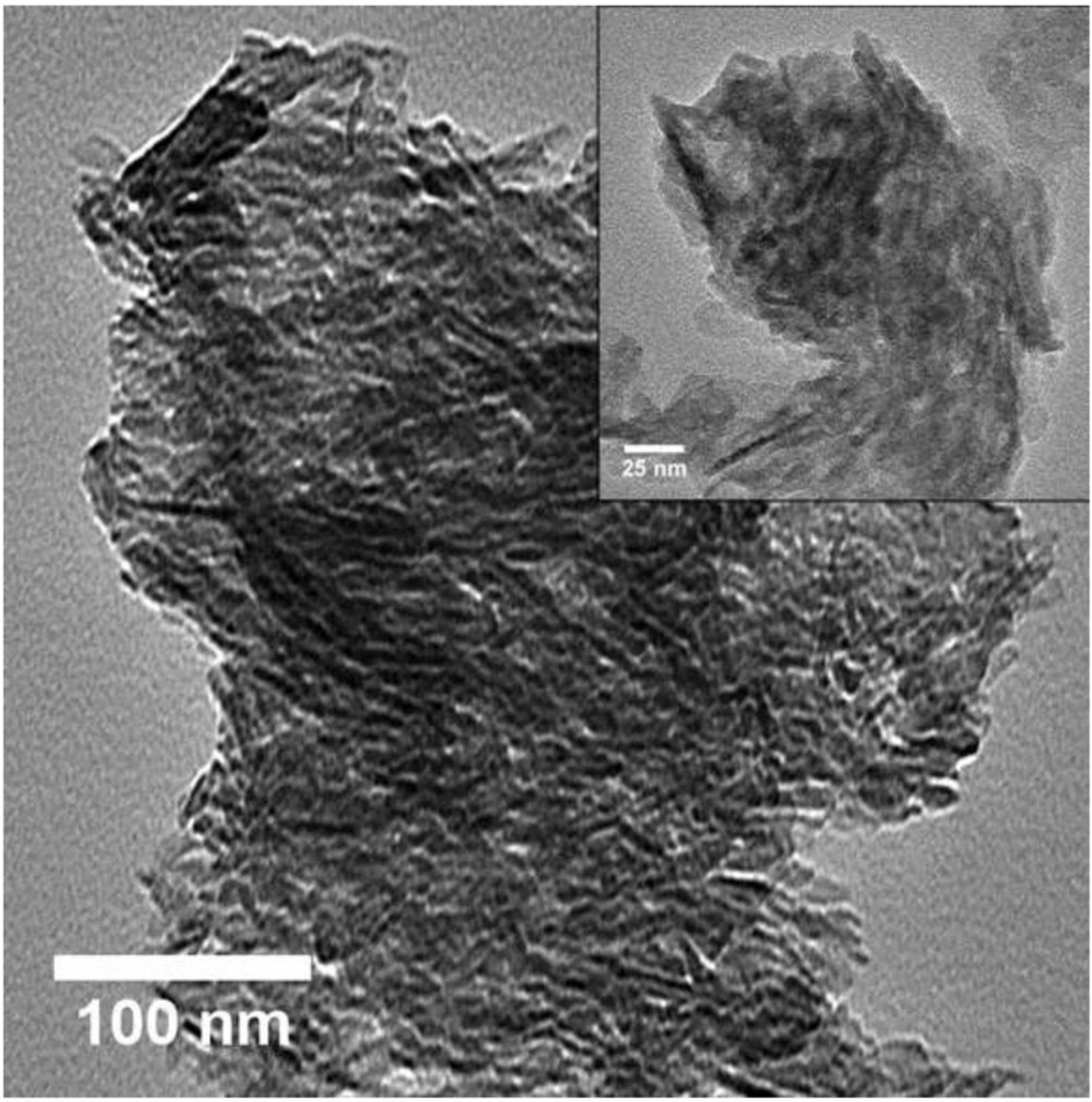

Fig. 6.

TEM images of (a) GEMOSIL-11 at 100 kx (inlet at 200 kx) and (b) GEMOSIL-19 at 100 kx (inlet at 200 kx) samples taken from the mixing step. Results confirm the integrity of the HAp-Gel nanocrystals where the needle shape crystals are embedded inside the matrix without damage. However, the GEMOSIL-11 sample shows more distinct needle shape crystals than GEMOSIL-19 sample, which is due to the lower amount of enTMOS coating layer.

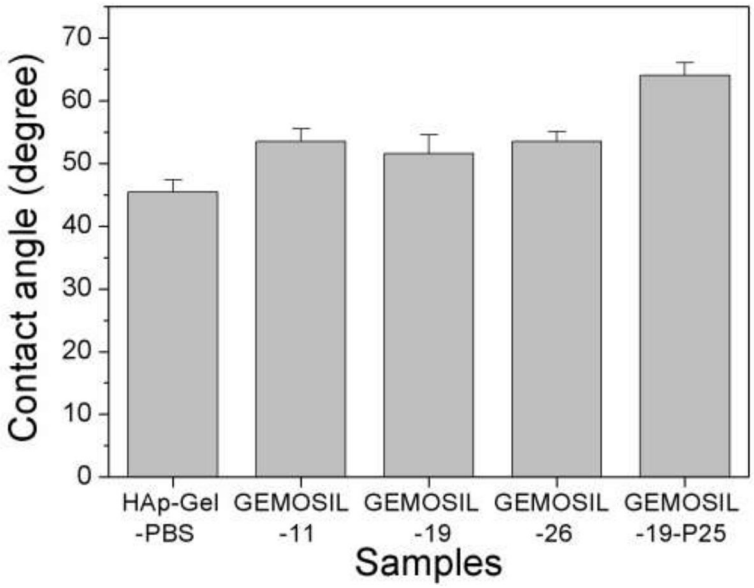

Fig. 7.

Contact angles measurements show no obvious difference between HAp-Gel-PBS and GEMOSIL samples. However, the addition of the TiO_2 (GEMOSIL-19-P25) increases the contact angle by about 10 degrees

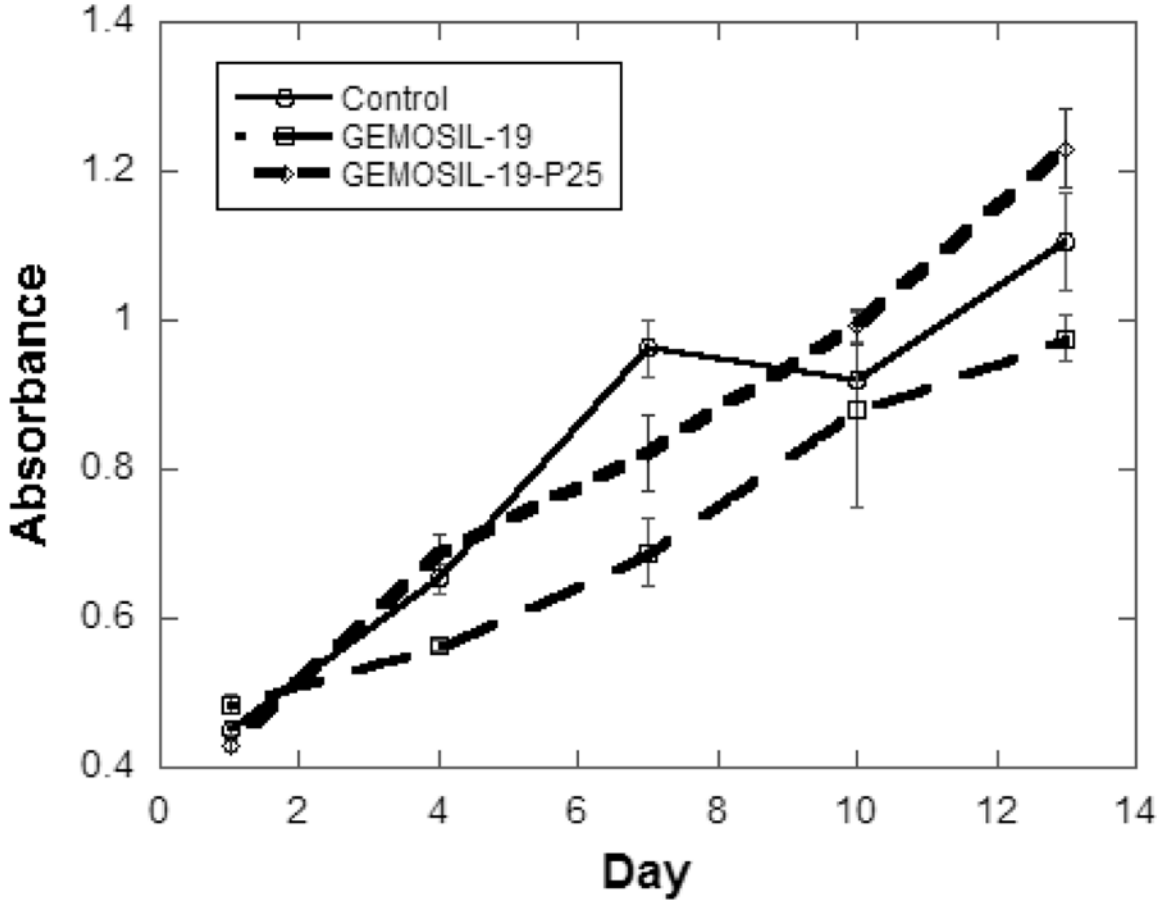

Fig. 8.

The growth curve of preosteoblasts, MC3T3-E1, was measured by formazan absorbance using CellTiter kits (Promega, Madison). There were significant differences among groups over time (1, 4, 7, 10 and 13 days) ($p < 0.05$)

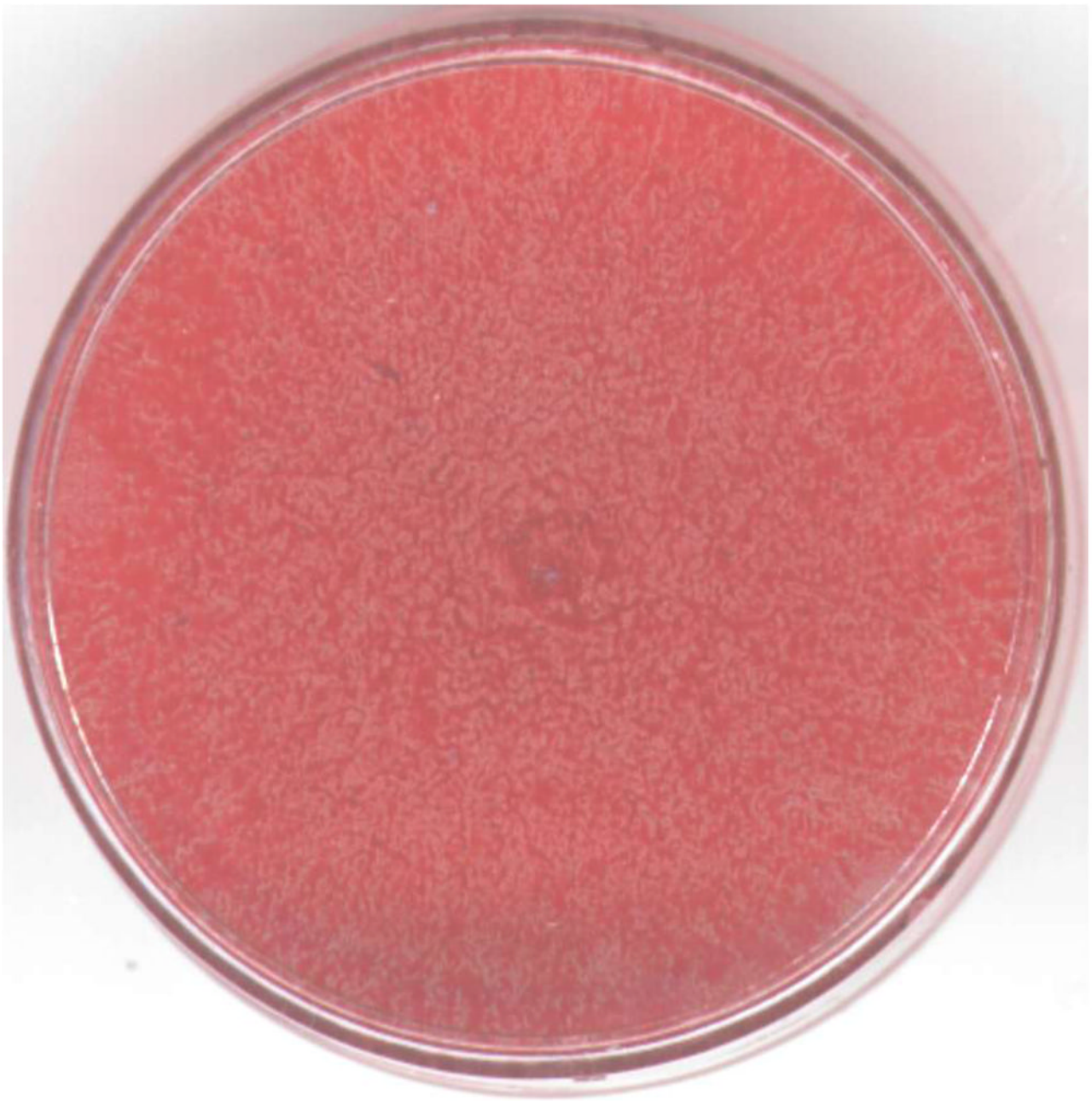

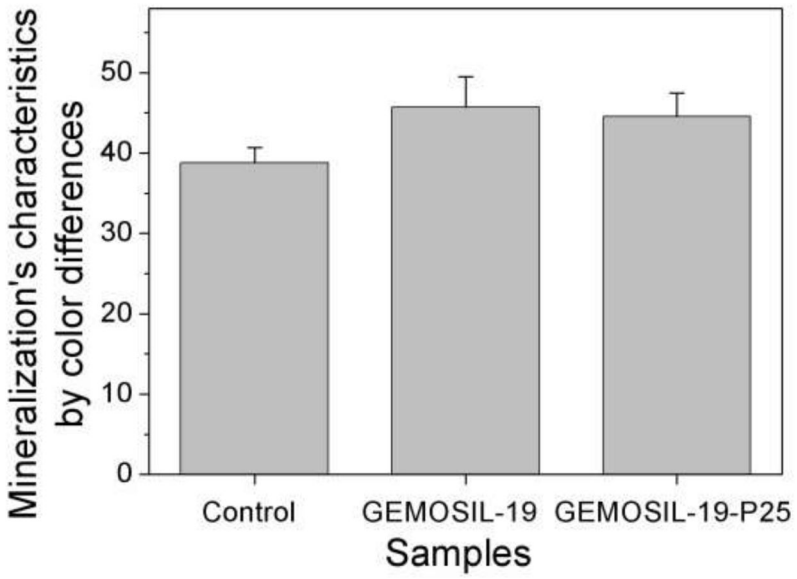

Fig. 9.

Alizarin red stain for MC3T3-E1 at the differentiation day 14 shows mineral nodules red for the (a) control. Both (b) GEMOSIL-19 and (c) GEMOSIL-19-P25 show abundant mineral stains covering the entire culture surface. (d) Quantification results of mineralization characteristics of control, GEMOSIL-19 and GEMOSIL-19-P25 derived from color differences (δ) by CIELAB method.

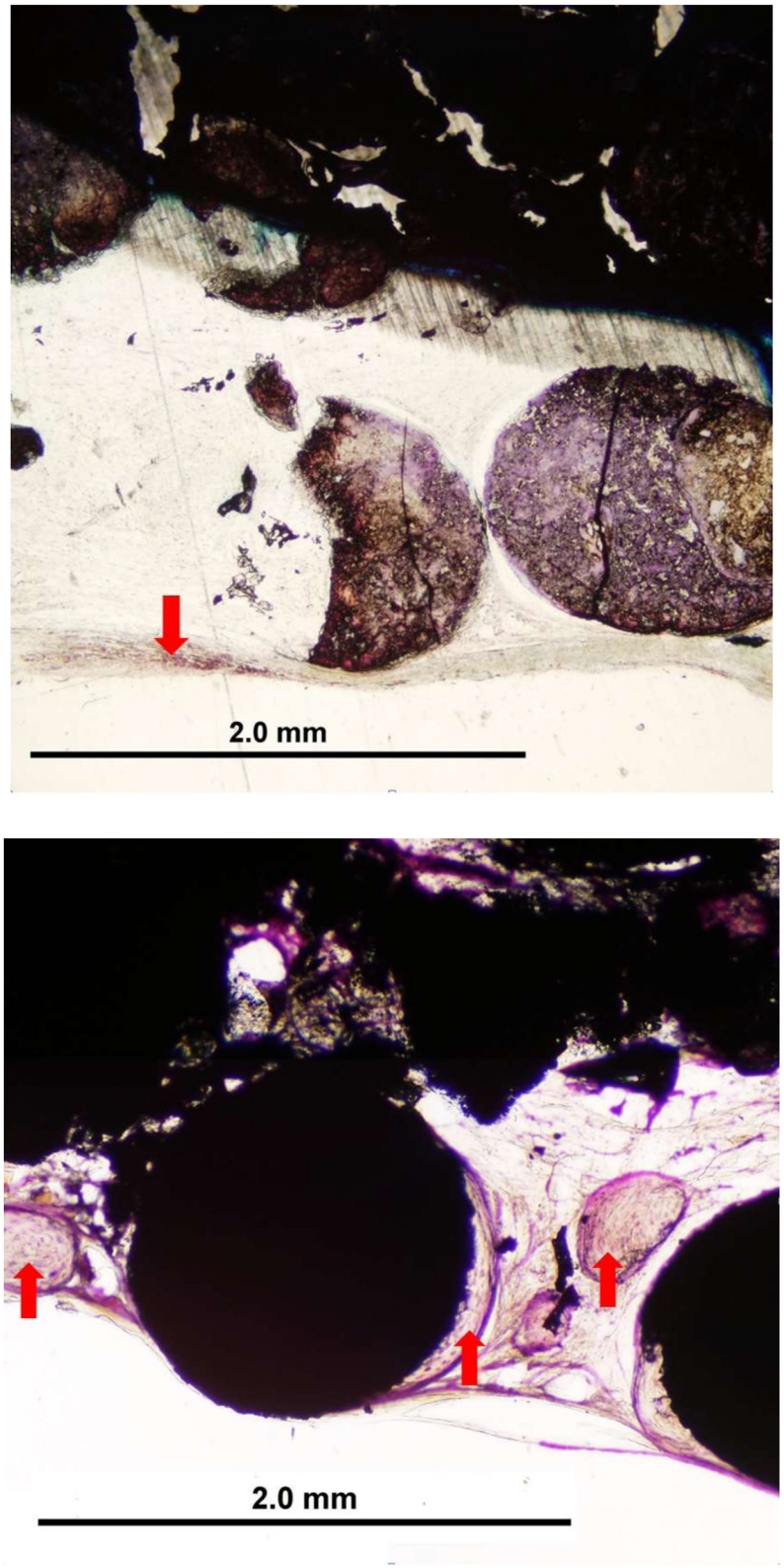

Fig. 10.

The rat calvarium defect study shows the new bone formation 8 weeks after implantation of the (a) GEMOSIL-19 and (b) GEMOSIL-19-P25

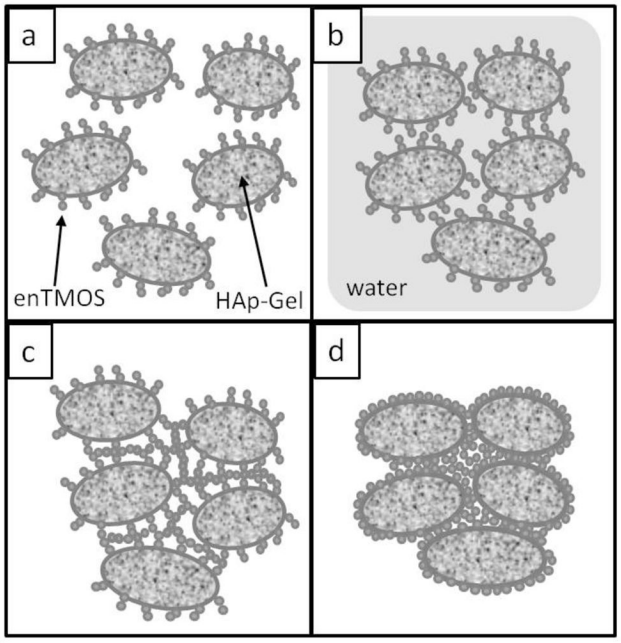

Sample	Notation code	HAp-Gel (mg)	enTMOS (μL)	PBS (μL)	P25 (mg)
1	HAp-Gel-PBS	400	0	800	0
2	GEMOSIL-11	400	48	800	0
3	GEMOSIL-19	400	96	800	0
4	GEMOSIL-26	400	144	800	0
5	GEMOSIL-19-P25	400	96	800	38

Fig. 11.

Setting mechanism for the GEMOSIL scaffold. (a) coating : hydrogen and chemical bonding begin to form between the thin enTMOS coating and HAp-Gel particles, (b) kneading : The hydrogen bonding provides the weak bonding and allowed short distance sliding among the HAp-Gel particles, which results in shapeable paste type properties and (c,d) hardening : solidification and particle packing start due to the gelation reaction and become strong monolith after aging and drying processes

Table 1

Composition of GEMOSIL nanocomposites

Sample	Notation code	HAp-Gel (mg)	enTMOS (μL)	PBS (μL)	P25 (mg)
1	HAp-Gel-PBS	400	0	800	0
2	GEMOSIL-11	400	48	800	0
3	GEMOSIL-19	400	96	800	0
4	GEMOSIL-26	400	144	800	0
5	GEMOSIL-19-P25	400	96	800	38